ACCOUNTS of chemical research

Article

pubs.acs.org/accounts

Structure–Property Relationships of Curved Aromatic Materials from First Principles

Laura Zoppi,[†] Layla Martin-Samos,[‡,§] and Kim K. Baldridge*,[†]

[†]Department of Chemistry, University of Zurich, Winterthurerstrasse 190, Zurich 8006, Switzerland

[‡]University of Nova Gorica, Materials Research Laboratory, vipavska cesta 11C, Ajdovscina 5270 Slovenia

[§]CNR-IOM DEMOCRITOS, Istituto Officina dei Materiali, c/o SISSA Scuola Internazionale Superiore di Studi Avanzati, Via Bonomea 265, 34136 Trieste Italy

CONSPECTUS: Considerable effort in the past decade has been extended toward achieving computationally affordable theoretical methods for accurate prediction of the structure and properties of materials. Theoretical predictions of solids began decades ago, but only recently have solid-state quantum techniques become sufficiently reliable to be routinely chosen for investigation of solids as quantum chemistry techniques are for isolated molecules. Of great interest are *ab initio* predictive theories for solids that can provide atomic scale insights into properties of bulk materials, interfaces, and nanostructures. Adaption of the quantum chemical framework is challenging in that no single theory exists that provides prediction of all observables for every material type. However, through a combination of interdisciplinary efforts, a richly textured and substantive portfolio of methods is developing, which promise quantitative predictions of materials and device properties as well as associated performance analysis.

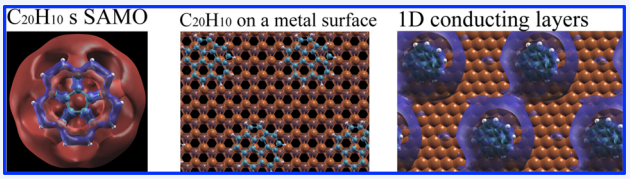

Particularly relevant for device applications are organic semiconductors (OSC), with electrical conductivity between that of insulators and that of metals. Semiconducting small molecules, such as aromatic hydrocarbons, tend to have high polarizabilities, small band-gaps, and delocalized π electrons that support mobile charge carriers. Most importantly, the special nature of optical excitations in the form of a bound electron–hole pairs (excitons) holds significant promise for use in devices, such as organic light emitting diodes (OLEDs), organic photovoltaics (OPVs), and molecular nanojunctions. Added morphological features, such as curvature in aromatic hydrocarbon structure, can further confine the electronic states in one or more directions leading to additional physical phenomena in materials. Such structures offer exploration of a wealth of phenomenology as a function of their environment, particularly due to the ability to tune their electronic character through functionalization.

This Account offers discussion of current state-of-the-art electronic structure approaches for prediction of structural, electronic, optical, and transport properties of materials, with illustration of these capabilities from a series of investigations involving curved aromatic materials. The class of curved aromatic materials offers the ability to investigate methodology across a wide range of materials complexity, including (a) molecules, (b) molecular crystals, (c) molecular adsorbates on metal surfaces, and (d) molecular nanojunctions. A reliable pallet of theoretical tools for such a wide array relies on expertise spanning multiple fields. Working together with experimental experts, advancements in the fundamental understanding of structural and dynamical properties are enabling focused design of functional materials. Most importantly, these studies provide an opportunity to compare experimental and theoretical capabilities and open the way for continual improvement of these capabilities.

■ INTRODUCTION

Design of new materials, such as organic light emitting diodes (OLEDs)[1] or organic photovoltaics (OPVs),[2] correlates with access to functional building blocks. Accurate prediction of the properties of structural arrays resulting from supramolecular ordering of building blocks requires consideration of dispersive effects, electronic correlation, and quantum confinement, and thereby naturally falls to first-principles approaches. However, this complexity of effects and typical building block sizes of greater than 20 heavy atoms creates a computational burden such that density functional theory (DFT) methods[3] become a favored theoretical tool.

DFT within the single-particle Kohn–Sham (KS) scheme,[3b] although remarkably accurate at times for description of ground state structures and properties of molecules and solids, fails for prediction of important properties such as noncovalent interactions[4] and HOMO–LUMO band gaps,[5] due to limitations imposed by approximate exchange and correlation (XC) functionals.[6] More advanced issues associated with electronic excitation processes introduce even more critical issues with the use of standard DFT methodology. Rigorously speaking, DFT provides an accurate description of total ground state electronic density only in the case of occupied KS states. Optical excitations[7] and charge-transfer[8] phenomena are at best poorly described within standard DFT, even with the most

Special Issue: DFT Elucidation of Materials Properties

Received: March 10, 2014
Published: June 16, 2014

   dx.doi.org/10.1021/ar5001132 | Acc. Chem. Res. 2014, 47, 3310–3320

accurate XC functionals available today, making benchmark accuracy across a wide array of materials properties a difficult task.[6]

The inherent challenge for first-principles based methodology is therefore not only establishment of a reliable pallet of methods, but also corresponding benchmark protocols for predictions. Ideally, methods should be equally accessible across a broad class of systems with comparable benchmark accuracy, including bulk materials, interfaces, and nanostructures. In this respect, the extended family of curved carbon π systems[9] are of particular interest as aromatic building blocks, which can be arranged in the solid state in varying complex environments.[10] As such, this class of systems provides an important opportunity for testing and optimizing existing, as well as new, theoretical methodology, for achieving a better comprehension of fundamental processes.

In this Account, the focus is on efforts to establish reliable theoretical approaches for prediction of structural, electronic, optical, and transport properties, as illustrated through a consistent class of materials systems based on curved aromatics, which as materials display a wide range of complexities. Curved aromatic components offer the prospect of a tunable spectrum of structure and electronic properties in connection with their morphology and dimensionality, as manifested through 0-D molecules, 3-D molecular crystals, 3-D organic−metallic surface interfaces, and 1-D organic nanojunctions.[9] Four illustrative cases are discussed: (1) superatom states of hollow molecules (SAMOs); (2) charge transfer excitations in molecular crystals; (3) molecular physisorption on metal surfaces; (4) electronic transport through a molecular nanojunction. Most importantly, these studies provide opportunities to compare methodology and avenues for improvements in theoretical capabilities.

SUPERATOM STATES (SAMOs) OF HOLLOW MOLECULES

As zero-dimension constructs, curved and spheroid aromatic compounds are ideal model systems for exploring nanomaterial properties. Carbon-rich organic molecules are appealing for devices due to their low density, structural stability, and extended π-networks. Interest in their use as active elements in nanoscale electronic devices and electron acceptor components of organic solar cells increases the need for better understanding of their fundamental electronic properties.[11] The ability to design and tune specific structural features provides an array of materials for testing and developing prototypes with unique electronic properties. Morphological features (e.g., curvature) can drastically affect orbital hybridization providing an avenue for fine-tuning of properties (e.g., electrical/optical band gap), and extended surface areas can be exploited for specialized reaction processes (e.g., catalysis), aggregated as monolayers supported on metallic surfaces, or aggregated as junctions for transport processes.[9]

Of particular relevance is experimental evidence of a characteristic set of diffuse molecular orbitals called super atomic molecular orbitals (SAMOs) in this class of molecules.[12] SAMOs are virtual orbitals that arise from the central potential of the molecular cavity, evoking well-defined hydrogenic s, p, and d orbital angular momentum shapes that extend beyond the molecule but are bound by a shallow potential at the center of the hollow structure.[12b] The diffuse nature of SAMOs gives rise to nearly free conducting channels when assembled in series in quantum nanostructures or solids.[12b,c] Unfortunately, prospects of exploiting the strong delocalization properties of SAMOs to achieve metal-like conduction in practical applications must be tempered by the fact that these orbitals are typically unoccupied.[12b,c]

The physical origin of SAMOs is ascribed to Many-Body screening and polarization effects, typical of a polarizable assembly (e.g., graphene) that undergoes a topological distortion, such as wrapping or rolling into a nanotube or fullerene.[12b,13] Polarization effects give rise to a series of degenerate image potential states (IP) in the near-surface region on both sides of a graphene sheet.[13] A topological distortion breaks symmetry, lowering or raising the energy of the IP states on the concave or convex side of the resulting material,[13] revealing SAMOs. Electron correlation effects inside the cavity manifest in an additional shallow attractive potential, resulting in significant electron density inside the cavity, unlike conventional Rydberg states that see the core as a point charge.

Taking a slightly different view from the typically studied spheroid fullerene, we have investigated the existence of SAMOs in a variety of symmetric bowl-shaped hollow molecules. Of particular interest is the bowl-shaped fullerene fragment corannulene ($C_{20}H_{10}$)[14] (Figure 1a,b), which is

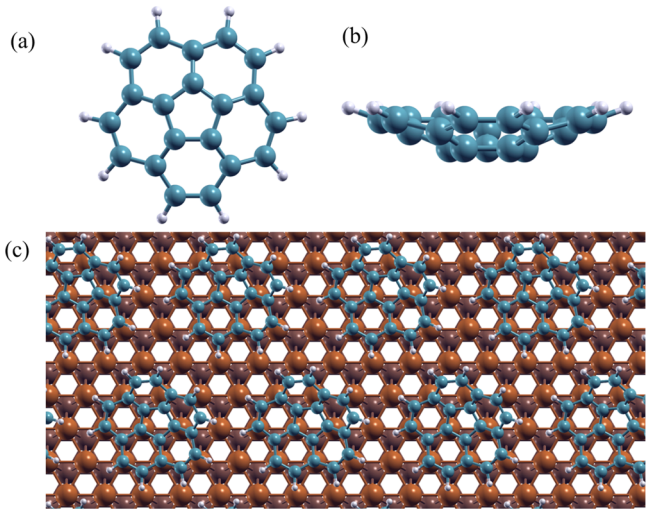

Figure 1. (a, b) $C_{20}H_{10}$ molecular structure; (c) $C_{20}H_{10}$ molecular layer supported on a Cu(111) surface.

extensively curved (bowl depth 0.9 Å), with large surface area and large intrinsic molecular dipole (2.1 D).[15,16] The ability to control curvature (and therefore reactivity and properties)[16] through functionalization of the rim,[17] together with the possibility of assembling these building blocks in layers on metallic surfaces,[10b,c,18] (Figure 1c), motivates their creative use as materials for supramolecular conducting layers.

Theoretical investigation of SAMOs requires methods that include Many-Body Perturbation Theory.[5a] We have customized a hybrid methodology based on plane-wave DFT formalism (Quantum-ESPRESSO)[19] and Many-Body Perturbation Theory (MBPT) in the GW approximation[20] (SAX).[21] The DFT wave function is used to initiate the solving of non-self-consistent Dyson-like equations for electronic screening and one particle electronic Green function.[20] The Dyson equation for the interacting Green function is written as

$$G = G^0 + G^0 \Sigma G \quad (1)$$

where G and G^0 are the interacting and noninteracting Green function, respectively, and the self-energy Σ plays the role of

dx.doi.org/10.1021/ar5001132 | Acc. Chem. Res. 2014, 47, 3310−3320

the exchange−correlation, XC, energy. Within the GW approximation,[5a,20] the self-energy is determined as the product of a single-particle Green function, G, and a nonlocal and dynamically screened Coulomb potential, W ($\Sigma = iGW$). One can still refer to single-particle energy levels; however, particles are quasi-particles (QP) renormalized for screening effects due to the presence of all other particles. GW and Hartree−Fock (HF) self-energies are very similar in that, in practice, the GW self-energy contains a HF term in addition to a pure polarization term, which includes the dielectric response of the electronic gas.[20b,22] In principle, the GW self-energy should be evaluated self-consistently. However, due to the high computational demands of such an approach, a non-self-consistent scheme, that is, G_0W_0,[23] with the initial G_0 obtained from DFT, is standard for practical calculations[5b,23] and is also the scheme adopted in this work. In this framework, exchange and Many-Body polarization effects critical for describing SAMOs properties are properly accounted for.

Figure 2a shows calculated SAMOs of corannulene, with the characteristic diffuse molecule-centered hydrogenic-like s, p, and d shapes, as typical of closed hollow structures such as C_{60}, which is also shown for comparison (Figure 2b).[12a] To exploit SAMOs in electron transport, one can imagine assembling a series of molecules on a metallic surface (e.g., Cu(111)).[24] In such a material, SAMOs would survive as delocalized electronic states, with the overlapping diffuse wave functions serving to facilitate electron transport (Figure 3).

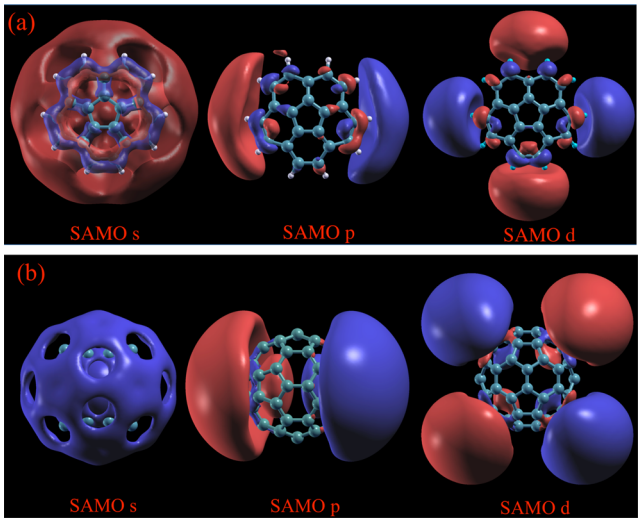

Figure 2. Single-point DFT calculation illustrating the 3D representation of SAMOs: typical s, p, and d-like symmetric shapes for (a) corannulene, $C_{20}H_{10}$, and (b) C_{60}.

To be relevant for transport, a SAMO either should be the first unoccupied state or should cross the Fermi level of the material such that occupation of the delocalized SAMOs can be enhanced. Thus, controlling the energy difference between lowest unoccupied molecular orbital (LUMO) and SAMO of lowest energy becomes quite useful. GW predictions of $\Delta E_{SAMO-LUMO}$ for isolated $C_{20}H_{10}$ are summarized in Table 1, with values for C_{60} shown for comparison. The SAMO level of s-type symmetry in both cases corresponds to the first unoccupied level after the LUMO. Notably, the $\Delta E_{SAMO-LUMO}$ energy gap for the SAMO orbital of s-type symmetry in $C_{20}H_{10}$ is predicted to be ∼0.3 eV, nearly an order of magnitude smaller than that for C_{60} (2.4 eV). One therefore expects

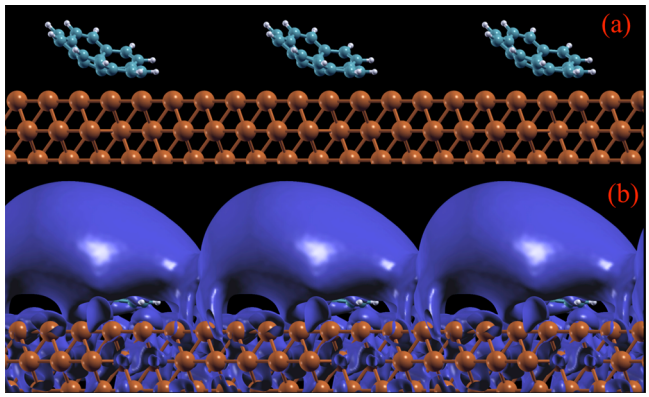

Figure 3. Single-point DFT calculation of $C_{20}H_{10}$ tiled onto a Cu(111) surface (a), illustrating the potential for SAMOs inter-interaction in the molecular layer (b).

Table 1. GW $\Delta E_{SAMO-LUMO}$ Values (in eV) for $C_{20}H_{10}$ and C_{60}

	$\Delta E_{SAMO-LUMO}$	
SAMO orbital type	$C_{20}H_{10}$	C_{60}
s	0.3	2.4
p	0.4	2.4
d	0.5	2.4

occupation of the delocalized SAMOs in $C_{20}H_{10}$, with the capacity to facilitate electron transport in a material using these bowl fragments as functional units.

A general strategy for reducing $\Delta E_{SAMO-LUMO}$ in a host cage, as previously shown for C_{60},[12b] consists of endohedral doping with electron-donating metals such as alkaline metals. This effectively enhances the central potential, causing the atomic and super atomic states to hybridize up to a limit where electron transfer from the metal to molecular LUMO can occur.[12b] In this respect, $C_{20}H_{10}$ has been shown to have strong electron-acceptor character and forms stable complexes with alkaline metals, accommodating up to four electrons in the doubly degenerate LUMOs.[10b] Photoelectron spectra and computation show complexes doped with Cs and deposited on a Cu(111) surface having full occupation of the original $C_{20}H_{10}$ degenerate LUMOs (Figure 4).[10b]

Possibilities for supporting $C_{20}H_{10}$−alkaline metal complexes on metallic surfaces hold promise for exploiting the diffuse nature of SAMOs in transport conducting layers. Cage-doping with metals having large ionization potentials (e.g., Li, Na) are the most effective for tuning the $\Delta E_{SAMO-LUMO}$ energy gap.[12b] Theory and experimental efforts are in progress to investigate SAMO properties across a series of $C_{20}H_{10}$−alkaline doped systems supported on metal surfaces, which should suggest possible experimental realizations of supramolecular conducting layers.

CHARGE TRANSFER EXCITATIONS IN MOLECULAR CRYSTALS

Organic semiconductors composed of π-conjugated systems typically absorb/emit in the UV−visible region and support electronic excitations in the form of bound electron−hole pairs (excitons).[25] These excitons can eventually recombine and either emit light (OLEDs) (Figure 5a) or further separate and conduct current (OPVs) (Figure 5b). Understanding structural and electronic modifications that drive transitions from

dx.doi.org/10.1021/ar5001132 | Acc. Chem. Res. 2014, 47, 3310−3320

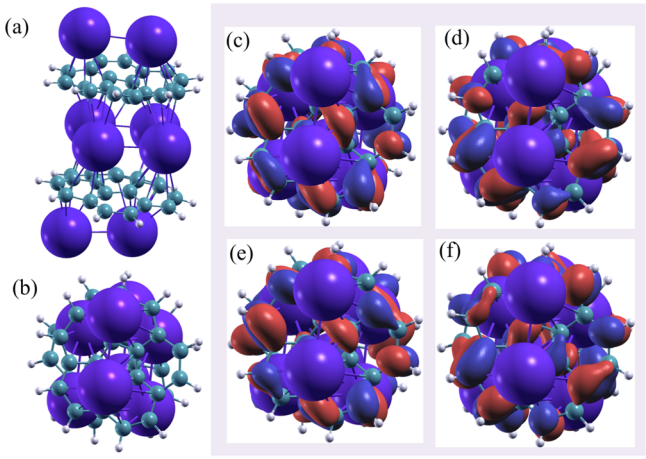

Figure 4. Side (a) and top (b) views of $(Cs_4{-}C_{20}H_{10})_2$ stacked dimer; (c–f) highest occupied orbitals of the dimer complex $(Cs_4{-}C_{20}H_{10})_2$ localized on $C_{20}H_{10}$ showing LUMO features of free corannulene.

photoinduced intramolecular (Frenkel) excitons to charge transfer (CT) states where electron and hole are spatially separated, and vice versa, is an important goal for improving functionality of OSC compounds.[26] While such modifications can have profound influence on carrier generation and loss mechanism in devices, the underlying physical chemistry is still poorly understood. Insight from theory into fundamental electronic processes driving the conversion between molecular photoexcitations and free charges is highly desirable.

Accurate description of electronic excitations in the form of excitons represents a challenge for theory, although promising approaches are being developed.[8a,27] Characterization of CT states is even more difficult. Among the possible strategies, constrained DFT (CDFT)[28] represents one approach to the problem. In the CDFT methodology, one defines an appropriate density functional together with a specific constraint on the charge density, thereby forcing localization of charge onto a particular fragment in a molecule.[28,29] While CDFT methodologies[28] can be computationally as efficient as nonconstrained-DFT and have been shown to provide in specific cases quite reasonable results,[8c,30] these methods do not take into account either the perturbing field generated by the light or the interaction between the electron and the hole. When an electron–hole couple is created by promotion of an electron into an unoccupied state, the two charge carriers cannot interact because the Hamiltonian depends only on the electronic density of the occupied states.

Standard time dependent DFT (TD-DFT)[5a,31] can qualitatively describe optical excitations with strong spatial overlap between involved occupied and unoccupied states. However, this method completely fails in describing weakly overlapping electron–hole pairs due to the lack of direct (attractive) interaction between electron and hole. Only if the underlying functional is fully nonlocal would TD-DFT be able to account for electron–hole direct interactions.[31a]

An alternative framework, considered state-of-the-art for characterizing excited states, consists of the solution of the Bethe–Salpeter equation (BSE), which belongs to the many body perturbation theory (MBPT) class, typically calculated within the GW approximation (GW-BSE).[5a] Such combined methodology is frequently used for investigations of bulk systems,[32] molecular crystals,[33] and 1D extended systems (e.g., nanowires).[34] Within this formalism, neutral excitation energies and optical spectra are obtained from solution of the BSE, which, using the GW data, accounts for electron–hole interactions.[5a] The BSE has a similar structure as single configuration interaction, except that the electron–hole interaction includes the information on the dielectric response of the electronic gas.[22]

In optical spectra, excitons appear as sharp transitions below the HOMO–LUMO band gap.[35] Key excited state results include full excitonic spectra with primary molecular states involved in the excitations and shape of excitonic wave functions. As documented in the literature, proper description of electronic structure within MBPT approaches is essential for accurately describing excited state properties of polyaromatic hydrocarbons. Key examples include studies involving polymeric systems and oligomeric chains, for example, polyacetylene, which was considered a protoype material for a long time,[35b,36] and pentacene, one of the most studied systems.[37] For assemblage of donor–acceptor systems, such as C_{60}/C_{70} as an acceptor and an organic molecule as a donor (pentacene, porphyrin), electron–hole interactions are a key component toward accurate predictability of the excitation properties.[8a,b] Nevertheless, although Many-Body techniques have been used since the mid-1980s, application to charge-transfer (CT)

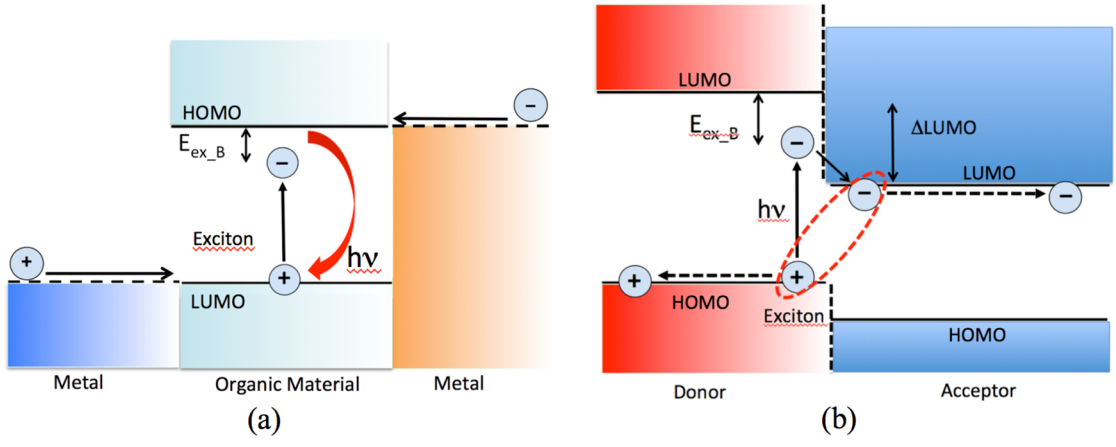

Figure 5. Schematic representation of excitons and exciton binding energy (E_{ex_B}) in (a) OLED multilayer material, where electrons and holes injected from opposite sides recombine and emit light and (b) OPV device with an organic donor–acceptor (DA) interface that facilitates the charge-separation process of the photogenerated electrons and holes.

dx.doi.org/10.1021/ar5001132 | Acc. Chem. Res. 2014, 47, 3310–3320

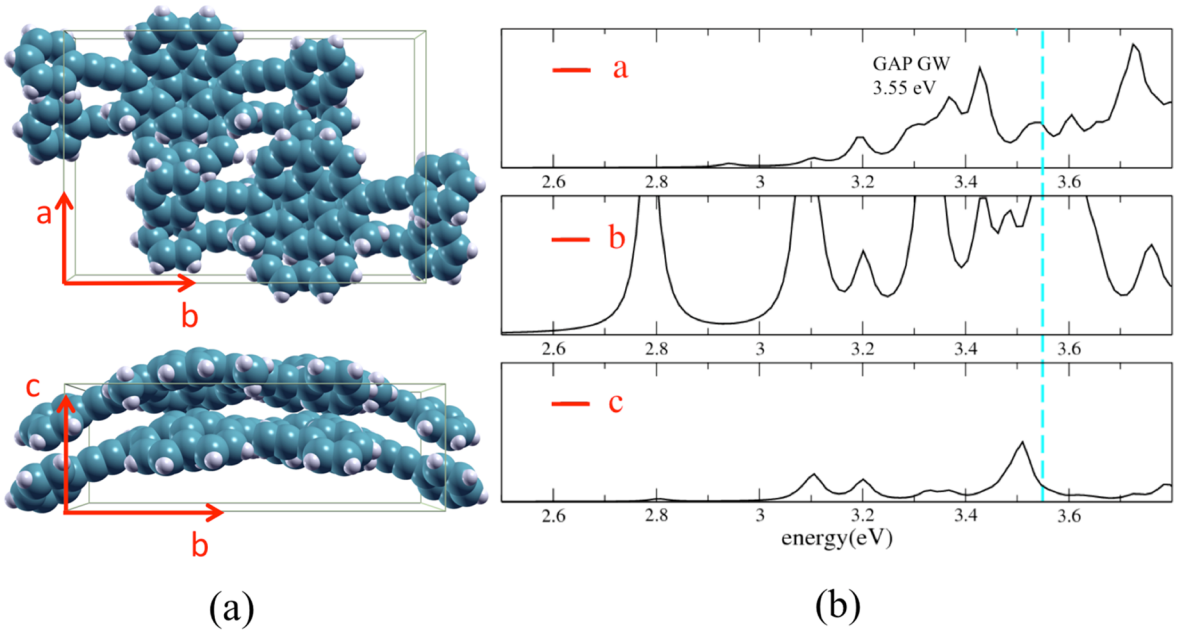

Figure 6. (a) Crystal structure of 1,6-diphenylethynylcorannulene and (b) GW-BSE-predicted optical absorption spectra along the three crystallographic directions (using an artificial Lorentzian broadening of 0.02 eV).

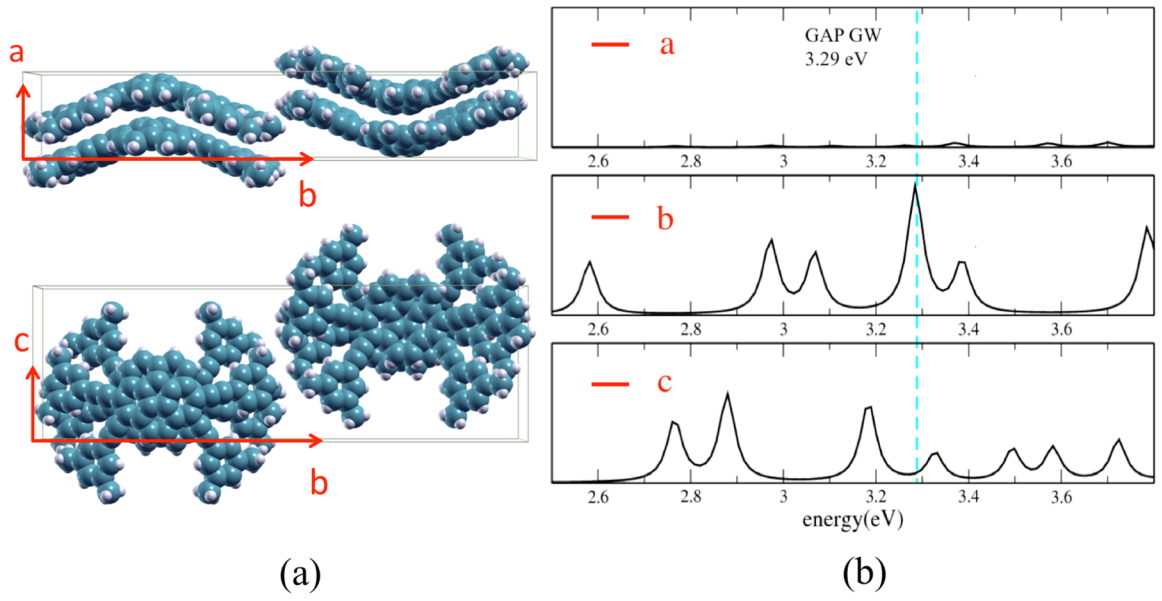

Figure 7. (a) Crystal structure of 1,2,5,6-tetraphenylethynylcorannulene; (b) GW-BSE-predicted optical absorption spectra along the three crystallographic directions (using an artificial Lorentzian broadening of 0.02 eV).

excitations in π-conjugated low dimensional systems still remains in its infancy. More extensive testing to establish strengths and limitations of customized and enhanced hybrid methodology will ultimately be of great value.[27]

Understanding potential applicability of organic materials in devices requires consideration of associated optical properties in the crystalline structure. The specific nature (Frenkel or CT) of excitons in the crystal requires knowledge of the optical absorption spectra, together with the exciton wave function in the different crystal packing forms. As motivating application in the present discussion, we illustrate the GW-BSE framework for investigation of an array of $C_{20}H_{10}$ derivatives, which have shown experimental promise of high quantum efficiency solution luminescence and variable emission wavelengths as a function of the nature and number of arm substituents.[10a,17] Interestingly, while the parent $C_{20}H_{10}$ does not display any particular columnar order, most functionalized derivatives show columnar arrangement along a particular stacking axis. For example, quite different columnar packing in the crystal is observed as a function of number of substituents in arylethynyl derivatives, such as 1,6-diphenylethynylcorannulene (Figure 6) and 1,2,5,6-tetraphenylethynylcorannulene (Figure 7).[17]

For electroluminescence purposes, sizable contribution of singlet states at the free electron−hole threshold (GW gap) in the optical absorption spectrum is an indication of the existence of light-coupled states available for recombination of injected electrons and holes that can afterward emit light (OLEDs).[1b] Calculated optical absorption spectra for 1,6-diphenylethynyl-

dx.doi.org/10.1021/ar5001132 | Acc. Chem. Res. 2014, 47, 3310−3320

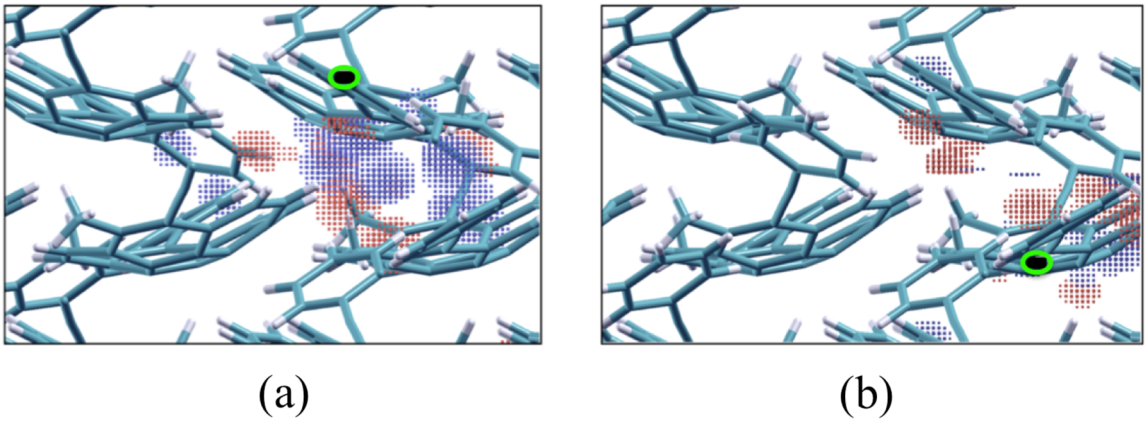

Figure 8. Exciton wave function corresponding to an energy of 3.54 eV in crystalline 1,6-diphenylethynylcorannulene for (a) electron (black rectangle, hole position) and (b) hole (black rectangle, electron position).

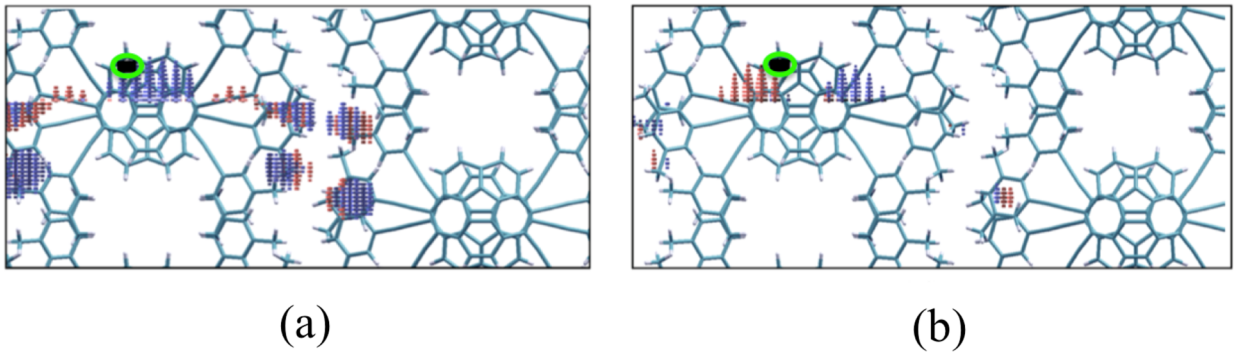

Figure 9. Exciton wave function corresponding to an energy of 3.28 eV in crystalline 1,2,5,6-diphenylethynylcorannulene for (a) electron (black rectangle, hole position) and (b) hole (black rectangle, electron position).

corannulene and 1,2,5,6-tetraphenylethynylcorannulene reveal important contributions of states along one or more of the three crystallographic directions in the region of the GW gap. For 1,6-diphenylethynylcorannulene, a major contribution of light-coupled states occurs along the *b* direction, coinciding with the axis of the long substituent arms. In 1,2,5,6-tetraphenylethynylcorannulene, one sees a large peak at the Fermi level occurring only along the *b* direction.

Given promising results in the crystal, we also investigated solid-state effects on the nature (Frenkel or CT) of the excitons, by looking at the shapes of the exciton wave functions for excitation energies close to the GW gap.[10a] In the disubstituted system (Figure 8a,b), electron and hole are spatially separated (CT exciton) with electron concentrated in the intramolecular space (Figure 8a) and hole concentrated on the molecular units (Figure 8b). The electron distribution suggests a "hopping" mechanism between the two molecular units along the stacking direction, indicating that a CT process can occur between molecules of the same column along the stacking direction. Together with the strong coupling with light in the optical absorption spectrum, this material holds promise for OLED performance.

A quite different view is observed for the tetra-substituted system, where electron and hole are localized on the same two submolecular units (Figure 9), with preference for two molecules pointing in the same direction, but in contrast to the previous system, they are not spatially separated, giving rise to a well-defined direct exciton. Crystal packing in which all molecules within the stacks face the same direction is most suitable for generating CT states and would be more effective for the purpose of OLED applications.

The most important advance in these investigations is the ability to predict the influence of packing effects on the nature of optical transitions in the crystal in conjugated organic molecules, where accurate and affordable theoretical methods are few.[5b,27] Such capability warrants investigation across a broader array of systems to fully establish performance of the combined GW method. This in turn should enable further theory advancements without resorting to approximation.

MOLECULAR PHYSISORPTION AND PAULI REPULSION

Understanding details of electronic transport across an interface between an active organic layer and a metallic surface is of considerable interest in the field of nanoscale electronics to enable better control in devices.[38] One important parameter governing electron transport at the metal−organic interface in organic device performance is the work function (WF).[39] In a bare metal surface, the inherent WF is a consequence of the intrinsic dipole caused by the spilling-out of electrons at the surface (Figure 10). For weakly bound adsorbates (e.g., most organic molecules), an additional dipole opposite to that of the metal surface is induced, termed the interface dipole (Figure 10).[40]

Characterization of molecules on surfaces represents a major challenge for standard DFT approaches, particularly due to the inability of current XC functionals to adequately describe long-range interactions, which constitute an important component

dx.doi.org/10.1021/ar5001132 | Acc. Chem. Res. 2014, 47, 3310−3320

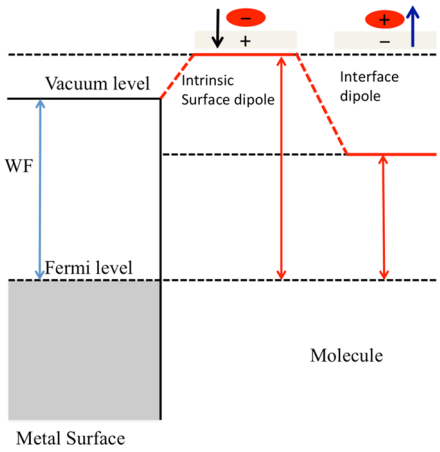

Figure 10. Schematic of surface WF (difference between vacuum level and Fermi level), dipole of a clean metal surface (intrinsic surface dipole), and induced dipole upon molecular adsorption (interface dipole).

of the adsorption process.[41] Recent progress to include vdW interactions within standard DFT include semiempirical dispersion corrections (DFT-D)[42] or fully first-principles vdW density functionals (vdW-DF).[4c] Both schemes have been successful in showing that the additional attractive interaction is crucial for determination of adsorption geometries, energetics, and associated force responsible in binding of molecules to a surface.[4d,e,41,43]

To improve organic-device performance, low WF interfaces, appropriate for electron transport at the metal−organic interface, must be tailored. Recently, deposition of $C_{20}H_{10}$ and functionalized $C_{20}H_{10}$ onto copper surfaces shows the possibility for tuning the molecule−organic interface WF.[24] For example, experiments establish that $C_{20}H_{10}$ and $C_{20}(CH_3)_5$ deposited on Cu(111) surface cause significant decrease in surface WF, up to 1.4 eV, with corresponding interface dipole of 8−9 D, without inducing appreciable charge transfer.[24] To understand details of the adsorption process, electronic structure analysis at the metal−molecule interface needs to be considered.

To model the adsorption process of $C_{20}H_{10}$ on Cu(111) surface, a six-layer Cu(111) slab (~400 atoms) with $C_{20}H_{10}$ approaching the surface was considered (Figure 11a,b).[10c] Corannulene approaches in a tilted bowl-up configuration, with one hexagonal ring sitting on top of a fcc hollow site. A dispersion-enabled localized orbital DFT strategy (SIESTA),[44] DFT-D, was used to investigate electronic structure and mechanistic details.[45] For the low coverage case of an isolated molecule on Cu(111) surface, the optimized structure

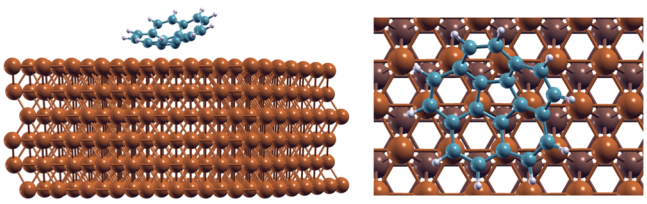

Figure 11. (a) $C_{20}H_{10}$ approaching a Cu(111) six-layer slab in a tilted bowl-up configuration and (b) $C_{20}H_{10}$ adsorption geometry with one hexagonal ring on top of a fcc hollow site.

established the hexagonal ring essentially parallel to and 2.2 Å above the copper surface.[45] In comparison, standard DFT without dispersion results in detachment of corannulene from the surface.

Mechanistic details at the interface clearly established a physisorption process governing the interaction between organic material and metallic surface,[45] balancing attractive vdW forces of the molecule to the surface and Pauli repulsion[40] from the electron spill-out of the metal (Figure 12).[40] Electrons

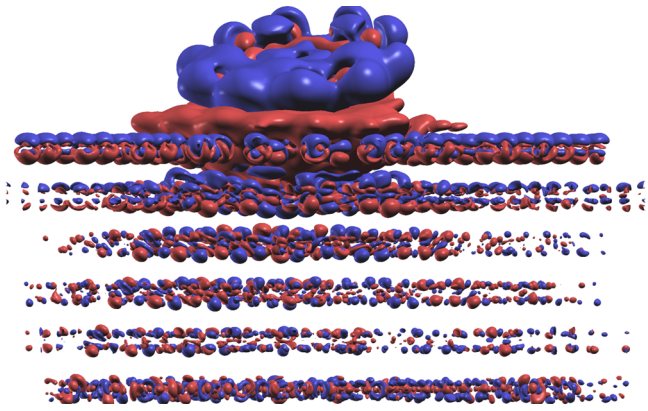

Figure 12. Depiction of charge density rearrangement of $C_{20}H_{10}$ approaching a Cu(111) surface. Blue, depletion of charge; red, accumulation of charge.

of the copper surface spill out above the surface atoms and are repelled down and sideways by $C_{20}H_{10}$. This push-back effect in the substrate, together with a notable depletion of charge in the molecular frame, induces substantial charge separation and a remarkable interface dipole (calcd 5.8 D; exptl 6.4−8.8 D). The consequence is a significant decrease in the surface WF (calcd ΔW = 1.37 eV; exptl 1.4 eV).[24,45] Pauli repulsion hinders overlap of the electronic wave function of the molecule with that of the metal, giving rise to the characteristic deformation of the surface electronic charge density, also known as the "cushion effect",[40] as illustrated in Figure 12.

Considering a more dense molecular packing requires accounting for depolarization effects from enhanced molecule−molecule dipolar interactions. This further affects the electronic structure at the interface.[46] Increasing surface coverage from 0.25 monolayers (ML) up to 1 ML (Figure 13b) shows an initial rapid linear increase of WF (in absolute value) with increasing coverage, followed by saturation (Figure 13a), in agreement with experiment.[24] The total dipole value of the complex decreases with increasing coverage, ranging from 5.8 D at ~0.25 ML to 3.4 D at 1 ML (Figure 13a).

In these studies, at both low and full monolayer coverage, theory clearly shows a physisorption phenomenon between the organic layer and metallic surface. Similar considerations with functionalized corannulene also show significant charge rearrangement at the interface with large interface dipole with significant decrease in WF, without any charge transfer. These investigations support and extend experimental efforts to shed light on adsorption mechanistics and offer valuable new ideas toward interface design for electrodes in electronic devices based on organic compounds.

dx.doi.org/10.1021/ar5001132 | Acc. Chem. Res. 2014, 47, 3310−3320

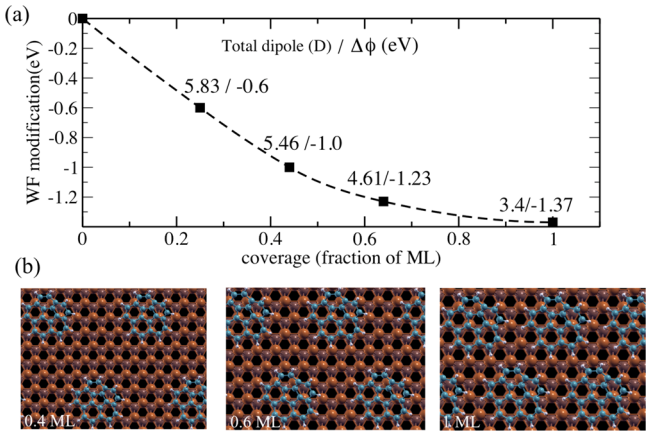

Figure 13. (a) Work function decrease ($\Delta\phi$) and total dipole versus increasing coverage (ML) for $C_{20}H_{10}$ adsorbed on Cu(111) and (b) varying surface coverage in terms of monolayers (ML).

ELECTRONIC TRANSPORT THROUGH MOLECULAR NANOJUNCTIONS

Devices in which organic molecules constitute the active element have attracted attention in the field of molecular electronics,[11] particularly with recent abilities to construct single-molecule junctions and measure their transport properties.[11,47] As conductor dimensions approach the nanoscale, design principles turn toward creation of molecules with tunable functionality in order to enable control of charge transport at the molecular scale.[11] In this respect, the extended family of curved aromatics based on $C_{20}H_{10}$ are key systems of interest, enabling design and construction of a variety of molecular building blocks with well-known structure−property relationships.[48] Their large intrinsic dipole can in principle govern molecular orientation under electrical stimulus when assembled into a molecular junction, resulting in interesting field-oriented materials properties.[15]

To explore fundamental static electronic response functions and electrical response properties under electrical stimulus, we investigated a series of increasingly curved molecules based on corannulene ($C_{20}H_{10}$−$C_{50}H_{10}$).[16] A DFT scheme based on a plane-wave and pseudopotential methodology (Quantum-ESPRESSO)[19] was compared with that of an all-electron localized basis description (GAMESS).[49] Calculated static polarizabilities across the series of buckybowls was used to derive a simple general analytical model describing the orientation of polarizable molecules under the influence of an external electric field.[16] Principal parameters of the model include polarizability components parallel and orthogonal to the intrinsic molecular dipole ($\alpha_{\|}$, $\alpha_{\perp}$), angle between the intrinsic dipole and the external electric field (ϑ), field intensity (E), and intrinsic dipole (P_0) (Figure 14). In linear response theory, total energy gain due to the presence of the field is

$$E_{tot} = -E_0\left[P_0 \cos\vartheta + \frac{1}{2}\alpha E_0 - \frac{1}{2}\alpha E_0 \cos^2\vartheta\right] \quad (2)$$

Model predictions for shallow bowls (e.g., $C_{20}H_{10}$) indicate that dipoles induced across the relatively large surface area of the cap region may become comparable to or larger than the intrinsic dipole, thereby governing the molecular orientation in the field.[16] Alternatively, for deeper bowls approaching tube-like structure, the magnitude of the polarizability along the

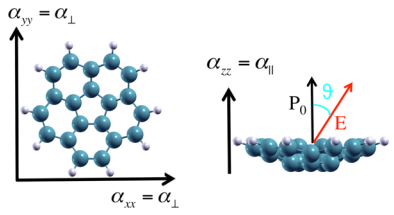

Figure 14. Analytical model parameters: electric field intensity (E), polarizability components parallel ($\alpha_{\|}$) and perpendicular ($\alpha_{\perp}$) to the intrinsic molecular dipole (P_0), and angle between intrinsic dipole and external field (ϑ).

molecular axis (z) aligns with the values along the x and y directions.[16]

To validate the analytical model predictions, *ab initio* calculations were performed on a model single-molecule junction, with $C_{20}H_{10}$ as the organic molecule linked to a (5,5)-nanotube fragment (Figure 15), including an electric

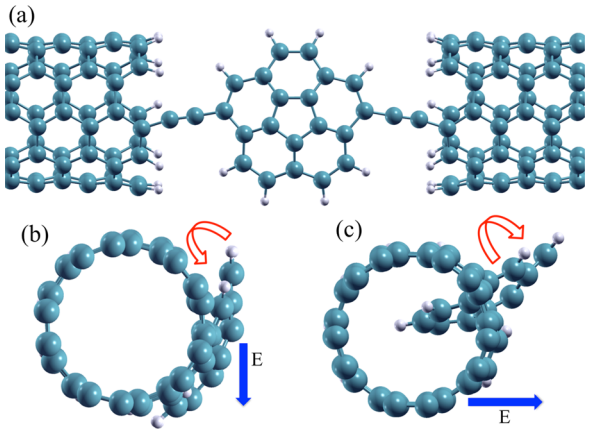

Figure 15. (a) Model junction structure, front view and (b, c) molecular rotations (red arrows) of the molecule inside the junction under the effect of an applied electric field (E, blue arrows). In both cases, the molecule rotates in accord with analytical model predictions.

field. The behavior of bowl fragment junctions in an electric field becomes key when exploiting response to electrical stimulus for governing orientation of the active element inside the junction. In a molecular switch, for example, conversion between two isomers must be controllable via external stimulus. Having the ability to control the direction of the switching process, such that conformation in the junction manifests two extreme configurations with significant on/off ratio for electronic transport, is useful for materials functionality.

Analytical model predictions of total energy upon molecular reorientation in the field indicate that energy gain due to field-induced molecular rotation is quite consistent. In the $C_{20}H_{10}$ junction, at a field strength of 0.006 Ha au, corannulene relaxes from an initial orientation with angle $\theta = 180°$ to field direction to a position having angle $\theta = 90°$ to field direction with energy gain of ~0.25 eV.[16]

In view of these findings, investigation of electron transport properties across a series of molecular junctions based on CNT/functionalized-$C_{20}H_{10}$/CNT nanojunction, with inclusion of electrical stimulus, is of interest. In principle, one could establish a switch using properties of the π network of the [CNT ↔ organic molecule junction ↔ CNT], with molecular orientation controlling preservation (on) or disruption (off) of

dx.doi.org/10.1021/ar5001132 | Acc. Chem. Res. 2014, 47, 3310−3320

the conjugated network. First-principles quantum conductance calculations are in progress to explore transport properties in the series to pose possible experimental realizations of such junctions.

CONCLUSIONS

This Account has dealt with developments made in recent years by this group to establish first-principles methodology for accurate theoretical description of electronic structure and properties of molecules and solids, as illustrated through applications of curved aromatic material systems. Given the failures in conventional DFT methods, we have customized coupled beyond-DFT methodologies that provide accurate structure, mechanistic, and excited state property details for curved aromatic based materials across a wide range of complexity. In conjunction with experiments, this pallet of theoretical protocols and associated analysis capabilities has enabled clarification of structural detail and physical/chemical mechanisms not fully understood at a fundamental level and thereby are shown to provide valuable insights into function in this class of materials.

The presented methodologies have already shown great potential for modeling device performances, as documented by several joint experimental−theoretical works recently appearing in the literature. In particular, first-principles quantum conductance calculations, in conjunction with experiment, have established quantum interference processes in molecular charge transport for π-conjugated molecules connected to metal electrodes.[50] Significant advancements have also been achieved in the case of donor−acceptor interfaces in OPV cells.[51] Here, the ability to describe photoinduced excitons, within prescribed MBPT[8a,b] and DFT-based techniques,[8c,51] is shown to be crucial for understanding electronic factors leading to unbound electron−hole charge separated states.

Clearly, much room exists for improvements in algorithmic efficiency, as well as breakthroughs to reduce the extent of approximations made in general. Continued work in these areas ultimately will extend predictive capabilities for advanced studies on materials phenomena and continue to push forth the frontiers of our knowledge in the area of functional materials.

AUTHOR INFORMATION

Notes

The authors declare no competing financial interest.

Biographies

Laura Zoppi received her Ph.D. in computational material science in 2003 at the University of Cagliari (Italy). Subsequently, she joined the Democritos National Simulation Center in Trieste as a postdoctoral fellow, followed by a second postdoctoral experience with Baldridge at UZH. She is currently Sr. Research Associate and lecturer at UZH.

Layla Martin-Samos received her Ph.D. in material science in 2004 at the University of Cergy-Pontoise (France). Subsequently, she joined the nanoSystems and nanoStructures at Surfaces National Center in Modena as a postdoctoral fellow. In 2008, she became Development Scientist at DEMOCRITOS and in 2012 joined the group of Valant at the University of Nova Gorica, where she is currently Assistant Professor.

Kim Baldridge received her Ph.D. in theoretical chemistry in 1988 at North Dakota State University (USA). She spent 15 years as Sr. Research Scientist and subsequent Director of Computational Science at the San Diego Supercomputer Center, with joint Professorship at the University of California, San Diego. She then transitioned to University of Zürich (UZH), where she has been Full Professor for over 10 years.

ACKNOWLEDGMENTS

We acknowledge the UZH-UFSP program and Swiss National Science Foundation for support of this research. CSCS is gratefully acknowledged for computer time.

REFERENCES

(1) (a) Uoyama, H.; Goushi, K.; Shizu, K.; Nomura, H.; Adachi, C. Highly efficient organic light-emitting diodes from delayed fluorescence. *Nature* **2012**, *492*, 234−240. (b) Friend, R. H.; Gymer, R. W.; Holmes, A. B.; Burroughes, J. H.; Marks, R. N.; Taliani, C.; Bradley, D. D. C.; Santos, D. A. D.; Brédas, J. L.; Lögdlund, M. Electroluminescence in conjugated polymers. *Nature* **1999**, *397*, 121−128.

(2) (a) Scharber, M. C.; Wuhlbacher, D.; Koppe, M.; Denk, P.; Waldauf, C.; Heeger, A. J.; Brabec, C. L. Design rules for donors in bulk-heterojunction solar cells - towards 10% energy-conversion efficiency. *Adv. Mater.* **2006**, *18*, 789−794. (b) Forrest, S. R. The path to ubiquitous and low-cost organic electronic appliances on plastic. *Nature* **2004**, *428*, 911−918.

(3) (a) Hohenberg, P.; Kohn, W. Inhomogeneous electron gas. *Phys. Rev.* **1964**, *136*, B864−B871. (b) Kohn, W.; Sham, L. Self-consistent equations including exchange and correlation effects. *Phys. Rev.* **1965**, *140*, A1133−A1138. (c) Dreizler, R. M.; Eberhard, E. K.; Gross, K. U. *Density Functional Theory: An Approach to the Quantum Many- Body Problem*; Springer-Verlag: Berlin, 1990.

(4) (a) Grimme, S.; Antony, J.; Schwabe, T.; Mück-Lichtenfeld, C. Density functional theory with dispersion corrections for supramolecular structures, aggregates, and complexes of (bio)organic molecules. *Org. Biomol. Chem.* **2007**, *5*, 741−758. (b) Antony, J.; Brüske, B.; Grimme, S. Cooperativity in noncovalent interactions of biologically relevant molecules. *Phys. Chem. Chem. Phys.* **2009**, *11*, 8440−8447. (c) Dion, M.; Rydberg, H.; Schröder, E.; Langreth, D. C.; Lundqvist, B. I. Van der Waals density functional for general geometries. *Phys. Rev. Lett.* **2004**, *92*, No. 246401. (d) McNellis, E. E.; Meyer, J.; Reuter, K. Azobenzene at coinage metal surfaces: Role of dispersive van der Waals interactions. *Phys. Rev. B* **2009**, *80*, No. 205414. (e) Atodiresei, N.; Caciuc, V.; Lazić, P.; Blügel, S. Chemical versus van der Waals interaction: The role of the heteroatom in the flat absorption of aromatic molecules C_6H_6, C_5NH_5, and $C_4N_2H_4$ on the Cu(110) Surface. *Phys. Rev. Lett.* **2009**, *102*, No. 136809.

(5) (a) Onida, G.; Reining, L.; Rubio, A. Electronic excitations: Density-functional versus Many-Body Green's-function approaches. *Rev. Mod. Phys.* **2002**, *74*, 601−659. (b) Rostgaard, C.; Jacobsen, K. W.; Thygesen, K. S. Fully self-consistent GW calculations for molecules. *Phys. Rev. B* **2010**, *81*, No. 085103. (c) Kaasbjerg, K.; Thygesen, K. S. Benchmarking GW against exact diagonalization for semiempirical models. *Phys. Rev. B* **2010**, *81*, No. 085102.

(6) Cohen, A. J.; Mori-Sánchez, P.; Yang, W. Challenges for density functional theory. *Chem. Rev.* **2012**, *112*, 289−320.

(7) Rohlfing, M.; Louie, S. G. Electron-hole excitations and optical spectra from first principles. *Phys. Rev. B* **2000**, *62*, 4927−4943.

(8) (a) Duchemin, I.; Blase, X. Resonant hot charge-transfer excitations in fullerene-porphyrin complexes: Many-Body Bethe-Salpeter study. *Phys. Rev. B* **2013**, *87*, No. 245412. (b) Baumeier, B.; Andrienko, D.; Rohlfing, M. Frenkel and charge-transfer excitations in donor−acceptor complexes from Many-Body Green's functions theory. *J. Chem. Theory Comput.* **2012**, *8*, 2790−2795. (c) Difley, S.; Voorhis, T. V. Exciton/charge-transfer electronic couplings in organic semiconductors. *J. Chem. Theory Comput.* **2011**, *7*, 594−601.

(9) Zoppi, L.; Siegel, J. S.; Baldridge, K. K. Electron transport and optical properties of curved aromatics. *Wiley Interdiscip. Rev.: Comput. Mol. Sci.* **2013**, *3*, 1−12.
(10) (a) Zoppi, L.; Martin-Samos, L.; Baldridge, K. K. Effect of molecular packing on corannulene-based materials electroluminescence. *J. Am. Chem. Soc.* **2011**, *133*, 14002−14009. (b) Bauert, T.; Zoppi, L.; Koller, G.; Siegel, J. S.; Baldridge, K. K.; Ernst, K.-H. Quadruple anionic buckybowls by solid-state chemistry of corannulene and cesium. *J. Am. Chem. Soc.* **2013**, *135*, 12857−12860. (c) Merz, L.; Parschau, M.; Zoppi, L.; Baldridge, K. K.; Siegel, J. S.; Ernst, K. H. Reversible phase transitions in a buckybowl monolayer. *Angew. Chem., Int. Ed.* **2009**, *48*, 1966−1969.
(11) Song, H.; Reed, M. A.; Lee, T. Single molecule electronic devices. *Adv. Mater.* **2011**, *23*, 1583−1608.
(12) (a) Feng, M.; Zhao, J.; Petek, H. Atomlike, hollow-core-bound molecular orbitals of C60. *Science* **2008**, *320*, 359−362. (b) Zhao, J.; Feng, M.; Yang, J. L.; Petek, H. The superatom states of fullerenes and their hybridization into the nearly free electron bands of fullerites. *ACS Nano* **2009**, *3*, 853−864. (c) Feng, M.; Zhao, J.; Huang, T.; Zhu, X.; Petek, H. The electronic properties of superatom states of hollow molecules. *Acc. Chem. Res.* **2011**, *44*, 360−368.
(13) Silkin, V. M.; Zhao, J.; Guinea, F.; Chulkov, E. V.; Echenique, P. M.; Petek, H. Image potential states in graphene. *Phys. Rev. B* **2009**, *80*, No. 121408.
(14) Borchardt, l.; Fuchicello, A.; Kilway, K. V.; Baldridge, K. K.; Siegel, J. S. Synthesis and dynamics of the corannulene nucleus. *J. Am. Chem. Soc.* **1992**, *114*, 1921−1923.
(15) Lovas, F. J.; McMahon, R. J.; Grabow, J.-U.; Schnell, M.; Mack, J.; Scott, L. T.; Kuczkowski, R. L. Interstellar chemistry: A strategy for detecting polycyclic aromatic hydrocarbons in space. *J. Am. Chem. Soc.* **2005**, *127*, 4345−4349.
(16) Zoppi, L.; Ferretti, A.; Baldridge, K. K. Static and field-oriented properties of bowl-shaped polynuclear aromatic hydrocarbon fragments. *J. Chem. Theory Comput.* **2013**, *9*, 4797−4804.
(17) Wu, Y.-T.; Bandera, D.; Maag, R.; Linden, A.; Baldridge, K. K.; Siegel, J. S. Multi-ethynyl corannulenes: Synthesis, structure and properties. *J. Am. Chem. Soc.* **2008**, *130*, 10729−10739.
(18) Parschau, M.; Fasel, R.; Ernst, K.-H.; Gröning, O.; Brandenberger, L.; Schillinger, R.; Greber, T.; Seitsonen, A. P.; Wu, Y.-T.; Siegel, J. S. Buckybowls on metal surfaces: Symmetry mismatch and enantiomorphism of corannulene on Cu(110). *Angew. Chem., Int. Ed.* **2007**, *46*, 8258−8261.
(19) http://qe-forge.org/gf/project/q-e/.
(20) (a) Hedin, L. New method for calculating the one-particle Green's function with application to the electron-gas problem. *Phys. Rev.* **1965**, *139*, A796−A823. (b) Hedin, L.; Lundqvist, S. *Effects of Electron-Electron and Electron-Phonon Interactions on the One-electron States in Solids*; Ehrenreich, H., Seitz, F., Turnbull, D., Eds.; Solid State Physics: Advances in research and Applications, Vol. *23*, Academic: New York, 1969.
(21) Martin-Samos, L.; Bussi, G. *Comp. Phys. Comm.* **2009**, *180*, 1416−1425.
(22) Fetter, A. L.; Walecka, J. D. *Quantum Theory of Many-Particle Systems*; McGraw-Hill: New York, 1971.
(23) Hüser, F.; Olsen, T.; Thygesen, K. S. Quasiparticle GW calculations for solids, molecules, and two-dimensional materials. *Phys. Rev. B* **2013**, *87*, No. 235132.
(24) Bauert, T.; Zoppi, L.; Koller, G.; Garcia, A.; Baldridge, K. K.; Ernst, K.-H. Large interface dipole moments without charge transfer: buckybowls on metal surfaces. *J. Phys. Chem. Lett.* **2011**, *2*, 2805−2809.
(25) Scholes, G. D.; Rumbles, G. Excitons in nanoscale systems. *Nat. Mater.* **2006**, 683−696.
(26) Barford, W. Theory of singlet exciton yield in light-emitting polymers. *Phys. Rev. B* **2004**, *70*, No. 205204.
(27) Rocca, D.; Lu, D.; Galli, G. Ab initio calculations of optical absorption spectra: Solution of the Bethe−Salpeter equation within density matrix perturbation theory. *J. Chem. Phys.* **2010**, *133*, 164109.
(28) Kaduk, B.; Kowalczyk, T.; Voorhis, T. V. Constrained density functional theory. *Chem. Rev.* **2012**, *112*, 321−370.
(29) Wu, Q.; Voorhis, T. V. Constrained density functional theory and its application in long-range electron transfer. *J. Chem. Theory Comput.* **2006**, *2*, 765−774.
(30) Yost, S. R.; Wang, L. P.; Voorhis, T. V. Molecular Insight Into the Energy Levels at the Organic Donor/Acceptor Interface: A Quantum Mechanics/Molecular Mechanics Study. *J. Phys. Chem. C* **2011**, *115*, 14431−14436.
(31) (a) Marques, M. A. L.; Ulrich, C. A.; Nogueira, F.; Rubio, A.; Burke, K.; Gross, E. K. U., *Time Dependent Density Functional Theory* Lecture Notes in Physics 706; Springer: Berlin, 2006. (b) Casida, M. E. Time-dependent density-functional theory for molecules and molecular solids. *J. Mol. Struct.: THEOCHEM* **2009**, *914*, 3−18.
(32) Albrecht, S.; Reining, L.; Sole, R. D.; Onida, G. Ab initio calculation of excitonic effects in the optical spectra of semiconductors. *Phys. Rev. Lett.* **1998**, *80*, 4510−4515.
(33) Hummer, K.; Ambrosch-Draxl, C. Oligoacene exciton binding energies: Their dependence on molecular size. *Phys. Rev. B* **2005**, *71*, No. 081202(R).
(34) Bruno, M.; Palummo, M.; Marini, A.; Sole, R. D.; Olevano, V.; Kholod, A. N.; Ossicini, S. Excitons in germanium nanowires: Quantum confinement, orientation, and anisotropy effects within a first-principles approach. *Phys. Rev. B* **2005**, *72*, No. 153310.
(35) (a) Rohlfing, M.; Louie, S. G. Electron-hole excitations in semiconductors and insulators. *Phys. Rev. Lett.* **1998**, *81*, 2312−2315. (b) Rohlfing, M.; Louie, S. G. Optical excitations in conjugated polymers. *Phys. Rev. Lett.* **1999**, *82*, 1959−1962.
(36) (a) Tiago, M. L.; Rohlfing, M.; Louie, S. G. Bound excitons and optical properties of bulk trans-polyacetylene. *Phys. Rev. B* **2004**, *70*, No. 193204. (b) Ferretti, A.; Mallia, G.; Martin-Samos, L.; Bussi, G. i.; Ruini, A.; Montanari, B.; Harrison, N. M. Ab initio complex band structure of conjugated polymers: Effects of hydrid density functional theory and GW schemes. *Phys. Rev. B* **2012**, *85*, No. 235105.
(37) (a) Tiago, M. L.; Northrup, J. E.; Louie, S. G. Ab initio calculation of the electronic and optical properties of solid pentacene. *Phys. Rev. B* **2003**, *67*, No. 115212. (b) Sharifzadeh, S.; Biller, A.; Kronik, L.; Neaton, J. B. Quasiparticle and optical spectroscopy of the organic semiconductors pentacene and PTCDA from first principles. *Phys. Rev. B* **2012**, *85*, No. 125307. (c) Sharifzadeh, S.; Darancet, P.; Kronik, L.; Neaton, J. B. Low-energy charge-transfer excitons in organic solids from first-principles: The case of pentacene. *J. Phys. Chem. Lett.* **2013**, *4*, 2197−2201. (d) Ambrosch-Draxl, C.; Nabok, D.; Puschnig, P.; Meisenbichler, C. The role of polymorphism in organic thin films: oligoacenes investigated from first principles. *New J. Phys.* **2009**, *11*, No. 125010.
(38) Neaton, J. B.; Hybertsen, M. S.; Louie, S. G. Renormalization of molecular electronic levels at metal-molecule interfaces. *Phys. Rev. Lett.* **2006**, *97*, No. 216405.
(39) Cahen, D.; Kahn, A. Electron energetics at surfaces and interfaces: Concepts and experiments. *Adv. Mater.* **2003**, *15*, 271−277.
(40) Witte, G.; Lukas, S.; Bagus, P. S.; Wöll, C. Vacuum level alignment at organic/metal junctions: 'Cushion' effect and the interface dipole. *Appl. Phys. Lett.* **2005**, *87*, No. 263502.
(41) Li, G.; Tamblyn, I.; Cooper, V. R.; Gao, H.-J.; Neaton, J. B. Molecular adsorption on metal surfaces with van der Waals density functionals. *Phys. Rev. B* **2012**, *85*, No. 121409.
(42) Grimme, S. J. Semiempirical GGA-type density functional constructed with a long-range dispersion correction. *J. Comput. Chem.* **2006**, *27*, 1787−1799.
(43) (a) Aradhya, S. V.; Frei, M.; Hybertsen, M. S.; Venkataraman, L. Van der Waals interactions at metal/organic interfaces at the single-molecule level. *Nat. Mater.* **2012**, *11*, 872−876. (b) Shi, X.-Q.; Li, Y.; Hove, M. A. V.; Zhang, R.-Q. Interactions between organics and metal surfaces in the intermediate regime between physisorption and chemisorption. *J. Phys. Chem. C* **2012**, *116*, 23603−23607.
(44) Soler, J. M.; Artacho, E.; Gale, D. J.; Garcia, A.; Junquera, J.; Ordejon, P.; Sanchez-Portal, D. The SIESTA method for ab initio order-N materials simulation. *J. Phys.: Condens. Matter* **2002**, *14*, 2745−2779.

(45) Zoppi, L.; Garcia, A.; Baldridge, K. K. Development of methods for computational analysis of the binding of molecules on metallic surfaces: Application to corannulene on copper surface. *J. Phys. Chem. A* **2010**, *114*, 8864−8872.
(46) Romaner, L.; Heimel, G.; Ambrosch-Draxl, C.; Zojer, E. The dielectric constant of self-assembled monolayers. *Adv. Funct. Mater.* **2008**, *18*, 3999−4006.
(47) Reed, M. A.; Zhou, C.; Muller, C. J.; Burgin, T. P.; Tour, J. M. Conductance of a molecular junction. *Science* **1997**, *278*, 252−254.
(48) Seiders, T. J.; Baldridge, K. K.; Grube, G. H.; Siegel, J. S. Structure/energy correlation of bowl depth and inversion barrier in corannulene derivatives: combined experimental, and quantum mechanical analysis. *J. Am. Chem. Soc.* **2001**, *123*, 517−525.
(49) Schmidt, M. W.; Baldridge, K. K.; Boatz, J. A.; Elbert, S. T.; Gordon, M. S.; Jensen, J. H.; Koseki, S.; Matsunaga, M.; Nguyen, K. A.; Su, S.; Windus, T. L.; Elbert, S. T. General atomic and molecular electronic structure system. *J. Comput. Chem.* **1993**, *14*, 1347−1363.
(50) (a) Guédon, C. M.; Valkenier, H.; Markussen, T.; Thygesen, K. S.; Hummelen, J. C.; Molen, S. J. v. d. Observation of quantum interference in molecular charge transport. *Nat. Nanotechnol.* **2012**, *7*, 305−309. (b) Vazquez, H.; Skouta, R.; Schneebeli, S.; Kamenetska, M.; Breslow, R.; Venkataraman, L.; Hybertsen, M. S. Probing the conductance superposition law in single-molecule circuits with parallel paths. *Nat. Nanotechnol.* **2012**, *7*, 663−667. (c) Aradhya, S. V.; Venkataraman, L. Single-molecule junctions beyond electronic transport. *Nat. Nanotechnol.* **2013**, *8*, 399−410.
(51) Congreve, D. l. N.; Lee, J.; Thompson, N. J.; Hontz, E.; Yost, S. R.; Reusswig, P. D.; Bahlke, M. E.; Reineke, S.; Voorhis, T. V.; Baldo, M. A. External quantum efficiency above 100% in a singlet-exciton-fission−based organic photovoltaic cell. *Science* **2013**, *340*, 334−337.